Enhanced Electrical Resistivity and Properties via Ion Bombardment of Ferroelectric Thin Films

*Sahar Saremi, Ruijuan Xu, Liv R. Dedon, Julia A. Mundy, Shang-Lin Hsu, Zuhuang Chen, Anoop R. Damodaran, Scott P. Chapman, Joseph T. Evans, and Lane W. Martin**

Defects are unavoidable in crystalline materials, and even in the most "perfect" materials there are always finite concentrations of various structural and compositional defects.[1] The presence of defects, in turn, can dramatically impact material properties; however, that impact is not always adverse and often the specific characteristics of materials can be engineered through controlled defect introduction. Semiconductor systems are an example in which defect engineering is extensively used to tailor properties. Years of development have gone into the production of large-scale, high-purity crystals with extremely low concentrations of grown-in defects.[2,3] These high-quality crystals, however, typically have limited utility in their pristine state and must be further processed to be used in devices. In fact, the wide-spread use of semiconductors in a range of applications is made possible by the finely-controlled and purposeful introduction of intrinsic and extrinsic defects which is accomplished through a variety of well-established techniques.[4]

Defect engineering in oxides, however, lags behind that in classic semiconductor systems due to the more complex nature of defects and difficulties in their characterization.[4] Add to this the fact that many complex oxides can accommodate large concentrations of defects and many atomic percent of non-stoichiometry prior to the formation of secondary phases,[5] and the complexity associated with controlling these materials becomes apparent. This said, like the classic semiconductor systems, even small concentrations of defects can induce dramatic changes in the electronic, dielectric, thermal, and other properties of oxides.[6–11] For example, in ferroelectric oxides, the presence of defects are regularly blamed for the degradation of performance by increasing leakage, reducing polarization, inducing fatigue, exacerbating aging, and prompting imprint.[6]

S. Saremi, R. Xu, L. R. Dedon, Dr. J. A. Mundy, S.-L. Hsu, Dr. Z. H. Chen, Dr. A. R. Damodaran, Prof. L. W. Martin
Department of Materials Science and Engineering
University of California
Berkeley, Berkeley, CA 94720, USA
E-mail: lwmartin@berkeley.edu
Dr. J. A. Mundy, S.-L. Hsu, Dr. Z. H. Chen, Prof. L. W. Martin
Materials Science Division
Lawrence Berkeley National Laboratory
Berkeley, CA 94720, USA
S. P. Chapman, J. T. Evans
Radiant Technologies, Inc.
2835 Pan American Fwy., Ste. B/C, Albuquerque, NM 87107, USA

DOI: 10.1002/adma.201603968

In turn, various defect-engineering strategies have been developed, including numerous chemical routes, which are designed to counteract the effects of or create specific defects to improve materials performance.[6,12–16] What has not been undertaken, however, is an approach akin to that applied in semiconductors wherein the properties of a material are deterministically altered by controlled introduction of specific defects in nearly perfect crystals such that we minimize those defects that detrimentally impact properties and introduce those that enhance the desired properties.

In this work we show how a defect-engineering method widely used in semiconductors can be implemented in complex-oxide ferroelectrics resulting in marked improvement of properties. Ion bombardment, which enables the controlled introduction of point defects and, in turn, tuning of the electrical properties of semiconductors,[17] enables production of specific regions of high resistivity on a wafer and allows one to isolate neighboring active device regions (hence the name "ion bombardment for isolation"). In such systems, ion bombardment is thought to produce defects which are associated with mid-gap states that act as traps and lead to semi-insulating behavior.[17] There has been similar work in complex oxides, wherein ion bombardment has been used to locally disrupt material properties.[18,19] Borrowing from these works, we explore a new approach for improvement of ferroelectric materials via controlled introduction of ion-bombardment-induced defects. In particular, we demonstrate that in the ferroelectric $PbTiO_3$, producing films with a high degree of crystallinity and chemical stoichiometry results in some of the least desirable properties (i.e., high leakage currents and losses) that would preclude such materials from use in any device. In turn, structural disorder and defects induced in situ by knock-on damage during growth or ex situ via ion bombardment can lower leakage currents by up to 5 orders of magnitude and improve the ferroelectric device performance. A combination of impedance spectroscopy, temperature-dependent current-voltage, and deep-level transient spectroscopy (DLTS) studies reveal no change in the conduction mechanism, but systematic changes in the trap energy from 0.24–0.27 eV in as-grown, pristine films to 0.93–1.01 eV for the ion-bombarded films which corresponds to a complete quenching of the shallow trap states. All told, the improved electrical performance is attributed to the formation of knock-on-damage induced defect complexes and clusters which produce deeper trap states and reduce free carrier transport. In turn, this approach shows that, akin to classic semiconductor materials, "pristine" materials are not always better and

© 2016 WILEY-VCH Verlag GmbH & Co. KGaA, Weinheim

controlled introduction of specific defect structures can be used to elicit the desired properties.

In this work, 140 nm $PbTiO_3$/20 nm $SrRuO_3$ thin-film heterostructures were grown on $SrTiO_3$ (001) single-crystal substrates (Crystec, GmbH) via pulsed-laser deposition (Experimental Section). We explore three growth variants for the $PbTiO_3$: (1) low-pressure, low-oxidative potential growth (50 mTorr oxygen; henceforth *low-pressure* O_2), (2) high-pressure, high-oxidative potential growth (200 mTorr oxygen; henceforth high-pressure O_2), and (3) high-pressure, low-oxidative potential growth (200 mTorr total pressure, 50 mTorr oxygen, balance argon; henceforth high-pressure O_2/Ar). Rutherford backscattering spectrometry (RBS) studies (Experimental Section) of heterostructure chemistry reveal that it is possible to produce essentially stoichiometric cation ratios, within the error of the RBS (±1%–2%), for all growth conditions simply by varying the laser repetition rate. In particular, we focus on films with measured stoichiometries of $Pb_{1.01}Ti_{1.00}O_x$ (low-pressure O_2), $Pb_{1.00}Ti_{1.00}O_x$ (high-pressure O_2), and $Pb_{1.01}Ti_{1.00}O_x$ (high-pressure O_2/Ar) (Figure S1, Supporting Information).

θ–2θ X-ray diffraction studies (**Figure 1**a) reveal that all heterostructures are epitaxial and single phase, but with marked differences in the crystalline quality of the various heterostructures. We note that the substrate and $SrRuO_3$ bottom electrode diffraction peaks are consistent and similar, regardless of the growth conditions of the top $PbTiO_3$. The low-pressure O_2 heterostructures (bottom, Figure 1a) exhibit relatively broad, low-intensity diffraction peaks which are slightly shifted to the left of their expected position (indicating a slightly expanded lattice parameter). On the other hand, the high-pressure O_2/Ar (middle, Figure 1a) and O_2 (top, Figure 1a) heterostructures exhibit high crystallinity as indicated by the presence of sharp, high intensity film peaks and two additional double-diffraction (Umweganregung) reflections[20] (at 24.01° and 45.08°)[21] which are only observed in highly crystalline heterostructures with coherent interfaces. The differences in crystalline quality are further supported by comparison of the full-width-at-half-maximum (FWHM) of the ω-scans (rocking curves) about the 002-diffraction condition of film and substrate (Figure 1b). For all heterostructures, the $SrTiO_3$ substrates are essentially identical (FWHM of 0.023°–0.026°). The high-pressure O_2 and O_2/Ar heterostructures exhibit relatively narrow rocking curves of 0.038° and 0.045°, respectively; indicating the excellent structural quality. The same analysis of the low-pressure O_2 heterostructures, however, reveals a full order of magnitude broader rocking curve (0.368°); indicative of considerably lower crystalline quality.

In order to study the properties of these films, symmetric $SrRuO_3$ capacitor structures were fabricated using established techniques (Experimental Section)[22] and dramatic differences were observed in the leakage characteristics of the

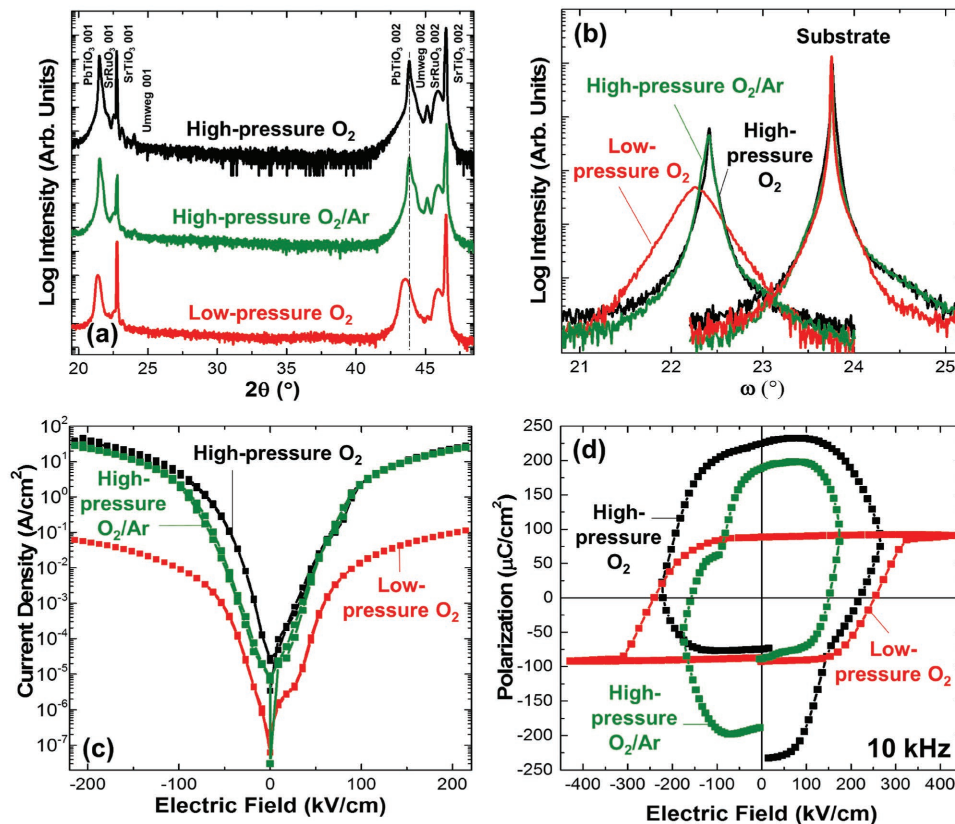

Figure 1. a) 2θ–ω X-ray diffraction scans of high-pressure O_2 (top), high-pressure O_2/Ar (middle), and low-pressure O_2 (bottom) heterostructures. b) Rocking curves about the 002-diffraction condition of film (left) and substrate (right) for high-pressure O_2 (FWHM = 0.038°), high-pressure O_2/Ar (0.045°), and low-pressure O_2 (0.368°) heterostructures; substrate rocking curves are also shown for comparison (FWHM = 0.023°–0.026°). c) Leakage current density as a function of DC electric field, and d) ferroelectric polarization-electric field hysteresis loops measured at 10 kHz for high-pressure O_2, high-pressure O_2/Ar, and low-pressure O_2 heterostructures.

© 2016 WILEY-VCH Verlag GmbH & Co. KGaA, Weinheim

heterostructures (Figure 1c). The high-pressure O_2 and O_2/Ar heterostructures reveal more than 2 orders of magnitude higher leakage current densities as compared to the low-pressure O_2 heterostructures. In turn, the high leakage current density of the heterostructures grown in high pressures precludes measurement of closed, saturated ferroelectric hysteresis loops, while nearly-square, fully saturated and closed hysteresis loops can be measured for the low-pressure O_2 heterostructures (Figure 1d).

This dramatic difference in crystalline quality, transport, and ferroelectric properties of the films grown at low- and high- pressures cannot be attributed simply to differences in stoichiometry. RBS studies revealed the films were nominally stoichiometric with respect to the cations. Furthermore, the high-pressure O_2/Ar heterostructures were produced at the same oxidative potential as the low-pressure O_2 heterostructures, but exhibit crystalline quality and properties akin to the high-pressure O_2 heterostructures, thus ruling out oxygen stoichiometry as a potential cause of the variations in crystalline quality and properties. We also note that ex situ anneals of the low-pressure O_2 heterostructures at 600 °C for 3 hours in 760 Torr of oxygen also resulted in no obvious changes to the structure, transport, or ferroelectric properties (Figure S2, Supporting Information). In turn, we propose that the differences between low- and high-pressure heterostructures stem mainly from the overall magnitude of the growth pressure, and hence from the difference in kinetic energy of the incoming adatoms. As the growth pressure is decreased, the adatoms undergo less scattering events in transit to the substrate and thus arrive with higher kinetic energy,[23,24] resulting in knock-on damage, and formation of structural defects (isolated point defects, complexes, or clusters), consistent with the expanded lattice parameter and low crystalline quality, which, in turn, could be responsible for reduction of the leakage and improvement of ferroelectric properties.

To explore this concept, a series of ex situ ion-bombardment experiments with varying bombardment doses (10^{14}–10^{16} cm^{-2}) were conducted on the high-pressure O_2 heterostructures. For these experiments, He^{2+} ions with an energy of 3 MeV were made incident across the entire sample (Experimental Section). SRIM (the stopping and range of ions in matter) and TRIM (transport of ions in matter) simulations (Experimental Section) suggest that lead, titanium, and oxygen vacancies are formed in the film as a result of bombardment, resulting in a defect concentration of the order of 10^{18}–10^{20} cm^{-3} for the dose range 10^{14}–10^{16} cm^{-2}. Furthermore, the high incident energy was chosen because the simulations suggest essentially no He^{2+} ions are implanted into the film, but instead the He^{2+} ions are stopped at an average depth of ≈13.5 µm, deep into the $SrTiO_3$ substrate (Figure S3, Supporting Information). RBS studies were completed before and after ion bombardment (Figure S4, Supporting Information), and reveal no change in the chemistry of the heterostructures for any dose studied herein. Increasing the irradiation dosage, however, does systematically worsen the crystalline quality of the heterostructures as manifested by a gradual increase of the FWHM of the rocking curve for the 002-diffraction condition from 0.0345° for the as-grown, high-pressure O_2 heterostructures to 0.1627° after a He^{2+} dose of 10^{16} cm^{-2} (**Figure 2**a). A slight expansion of out-of-plane

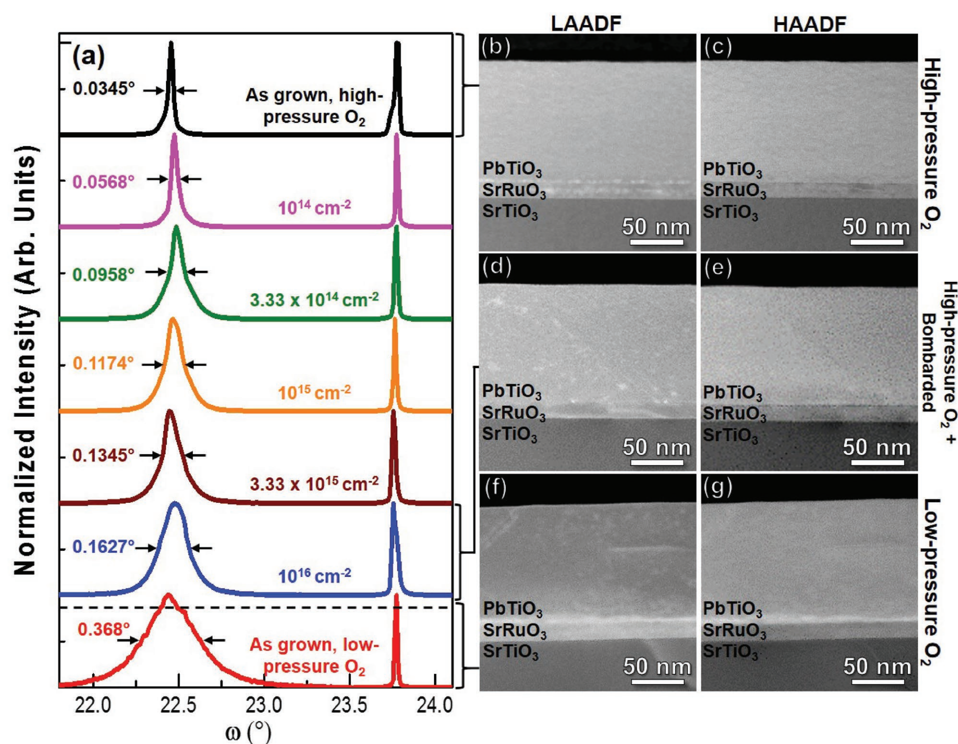

Figure 2. a) Rocking curves of a high-pressure O_2 heterostructure as a function of He^{2+} bombardment dose obtained about the 002-diffraction condition; the bottom rocking curve is for a low-pressure O_2 heterostructure for comparison. Low-angle annular dark field (LAADF-STEM) and high-angle annular dark field (HAADF-STEM) scanning transmission electron microscopy images of b,c) as-grown, high-pressure O_2, d,e) He^{2+} bombarded, high-pressure O_2 (dosage of 10^{16} cm^{-2}), and f,g) low-pressure O_2 heterostructures, respectively.

© 2016 WILEY-VCH Verlag GmbH & Co. KGaA, Weinheim

lattice parameter is also observed upon ex situ bombardment of the high-pressure O_2 heterostructures similar to what was observed in the in situ bombarded heterostructures (Figure S5, Supporting Information). It appears that the ex situ bombardment of a highly crystalline, high-pressure O_2 heterostructure can make it exhibit a similar crystallinity – or lack thereof – to the in situ bombarded, low-pressure O_2 heterostructures.

To further confirm the similarities between in situ and ex situ bombarded heterostructures, high-angle annular dark-field scanning transmission electron microscopy (HAADF-STEM) and low-angle annular dark-field STEM (LAADF-STEM) studies were completed. The HAADF-STEM provides chemical information in the form of *Z*-contrast, while LAADF-STEM is additionally sensitive to structure or anything that dechannels the transiting electrons (e.g., phonons or strain fields from point defects).[25,26] Examination of the high-pressure O_2 heterostructures reveals uniform contrast in both the LAADF-STEM and HAADF-STEM images suggesting uniform structure and chemistry and minimal defect density (Figure 2b,c). Following the ex situ bombardment (dosage of 10^{16} cm^{-2}), however, these heterostructures are found to change dramatically wherein LAADF-STEM images show the formation of splotchy contrast likely due to the formation of point defects and clusters (Figure 2d),[27] although no Z-contrast is observed in HAADF-STEM images. Finally, the LAADF-STEM images (Figure 2f) of the low-pressure O_2 heterostructures exhibit similar splotchy patterns to the ion-bombarded heterostructures, again with no *Z*-contrast in HAADF-STEM images (Figure 2g) suggesting that the bombardment from the in situ high-energy adatoms and that from the ex situ He^{2+} bombardment produce similar defect types.

The ex situ He^{2+} bombardment also has a similar effect to the in situ bombardment at low pressures on the transport and ferroelectric properties of the heterostructures. Increasing He^{2+} dosage systematically decreases the leakage current density of the heterostructures grown at high pressures by up to 5 orders of magnitude (**Figure 3**a), concurrent with lowering the crystalline quality of the films. As a result of this reduction of leakage, fully saturated ferroelectric loops with saturation polarization of ≈78 µC cm^{-2} (similar to that of the low-pressure O_2 heterostructures) are obtained in the dose range of 3.33×10^{15}–1.00×10^{16} cm^{-2} (Figure 3b).This further supports the idea that formation of knock-on-damage-related defects is responsible for lower leakage in the in situ and ex situ bombarded heterostructures as compared to the "pristine" high-pressure heterostructures.

To better understand the mechanism for the dramatic changes in electrical leakage, we have leveraged an array of characterization techniques. First, impedance spectroscopy (Experimental Section) provides a way to differentiate between various contributions to the overall resistive response. Nyquist impedance plots can contain several semicircles wherein each semicircle is characteristic of a single time constant or transport mechanism.[28,29] Impedance studies of the high-pressure O_2, low-pressure O_2, and He^{2+} bombarded, high-pressure O_2 (dosage of 10^{16} cm^{-2}) heterostructures were undertaken (Figure 3c). In all cases, only a single semicircle was observed; suggesting a single transport mechanism dominated by the bulk of the film. The magnitude of resistance (extracted from the intercept of the semicircles on the real axis), however, was found to vary greatly from 1.96×10^8 to 8.75×10^{10} to 1.76×10^{12} Ω for the high-pressure O_2, low-pressure O_2, and He^{2+} bombarded, high-pressure O_2 (dosage of 10^{16} cm^{-2}) heterostructures.

Having established that the transport remains bulk mediated, we proceeded to understand the origin of the large differences in the conductivity by applying both DLTS and temperature-dependent current–voltage (*I*–*V*) measurements (Experimental Section and Supporting Information). DLTS measurements can be used to probe a variety of trap states present in a material[30] while *I*–*V* studies can be used to reveal the dominant trap states and conduction mechanisms. DLTS data (i.e., the difference in transient capacitance at two different times t_1 and t_2 after a filling pulse) were obtained for five different rate windows at temperatures from 100 to 425 K (**Figure 4**a–c) and the activation energy of each trap state can be extracted from the shift of the DLTS peaks with temperature (Figure S6, Supporting Information). In the case of the high-pressure O_2 heterostructures (Figure 4a), two peaks can be observed indicating the presence of two different defect states

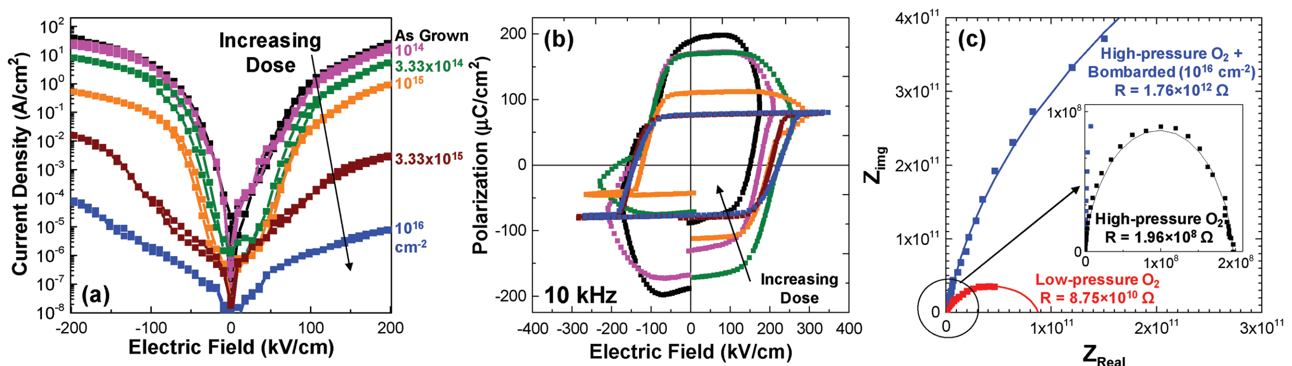

Figure 3. a) Leakage current density as a function of DC electric field for a high-pressure O_2 heterostructure which is progressively He^{2+} bombarded with the noted dosages. b) Ferroelectric polarization-electric field hysteresis loops measured at 10 kHz for the same high-pressure O_2 heterostructures after various He^{2+} bombardment doses. c) Nyquist plots (Z_{Img} vs. Z_{Real}) for as-grown, high-pressure O_2, He^{2+} bombarded, high-pressure O_2 (dosage of 10^{16} cm^{-2}), and low-pressure O_2 heterostructures. The presence of one semicircle in all of these heterostructures reveals a single transport mechanism while the magnitude of resistance (extracted from the intercept of the semicircles on the real axis) varies as noted.

© 2016 WILEY-VCH Verlag GmbH & Co. KGaA, Weinheim

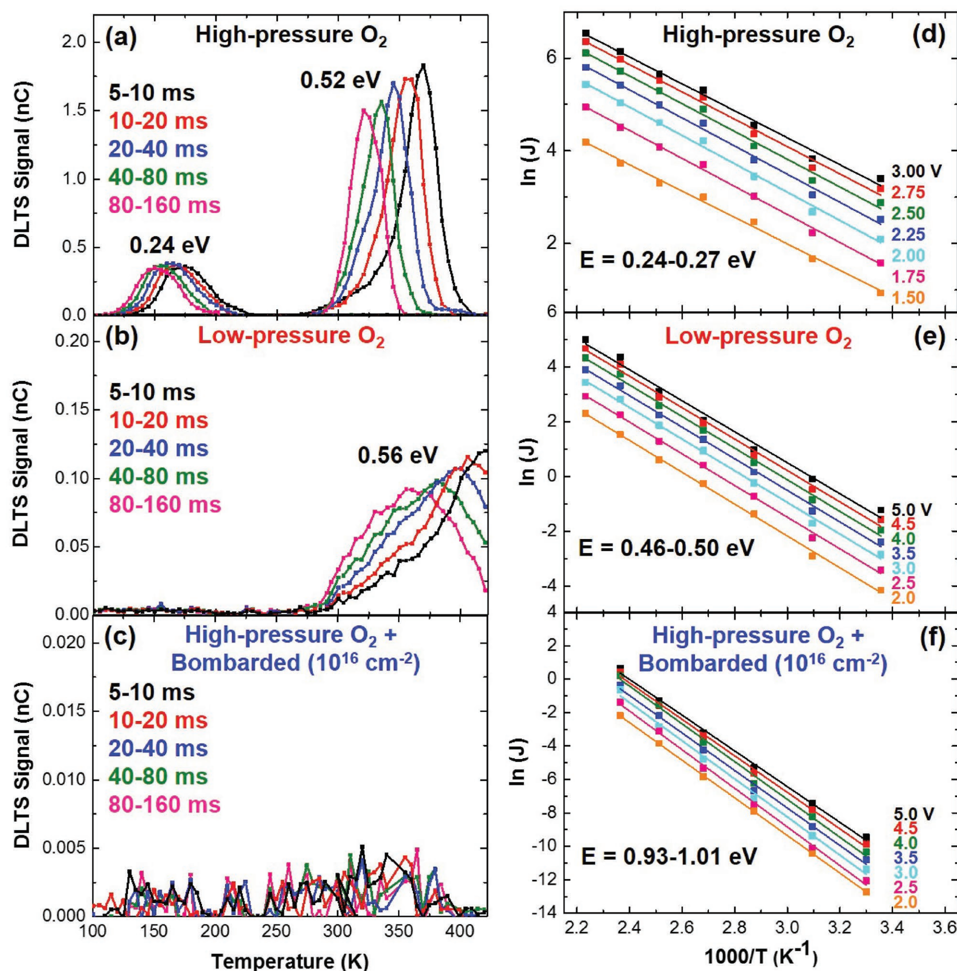

Figure 4. DLTS signal measured at five different time windows for a) high-pressure O_2, b) low-pressure O_2, and c) He^{2+} bombarded, high-pressure O_2 (dosage of 10^{16} cm^{-2}) heterostructures. Arrhenius plots of ln (J) versus 1000/T at different electric fields for d) high-pressure O_2, e) low-pressure O_2, and f) He^{2+} bombarded, high-pressure O_2 (dosage of 10^{16} cm^{-2}) heterostructures. The activation energies (noted) are extracted from the slope of the linear fits.

with activation energies of 0.24 and 0.52 eV. The difference in the intensity of the peaks indicates a higher concentration of the deeper trap state. For the low-pressure O_2 heterostructures (Figure 4b), only a single high-temperature peak was observed corresponding to an activation energy of 0.56 eV albeit with a much lower intensity compared to the similar peak in the high-pressure O_2 heterostructures. Moreover, this high-temperature peak in the in situ bombarded low-pressure O_2 heterostructures is broader and shifted in temperature compared to the same peak in the high-pressure O_2 heterostructures. Broadening of DLTS peaks is usually attributed to the formation of defect clusters which can give rise to a distribution in emission energy of the defect, while shifts of a peak can be caused by changes in the environment surrounding the defect or the defect configuration.[31,32] Finally, no DLTS signal could be measured for the He^{2+} bombarded, high-pressure O_2 heterostructures (Figure 4c) within the same temperature and time windows.

I–V measurements were carried out in order to identify the dominant conduction mechanism and trap state in each heterostructure. For the high-pressure O_2, low-pressure O_2, and He^{2+} bombarded, high-pressure O_2 (dosage of 10^{16} cm^{-2}) heterostructures, Poole–Frenkel emission was identified as the dominant conduction mechanism at fields >100 kV cm^{-1} (Figure S7a–c, Supporting Information). *I–V* response was obtained at different temperatures (Figure S7d–f, Supporting Information), and the activation energies were extracted for different applied electric fields (Figure 4d–f). From these fits, the dominant trap states were found to have activation energies of 0.25–0.27, 0.46–0.50, and 0.93–1.01 eV for the high-pressure O_2, low-pressure O_2, and He^{2+} bombarded, high-pressure O_2 (dosage of 10^{16} cm^{-2}) heterostructures, respectively.

These results can be understood by examining the nature of conduction and defects in these materials. The conduction in $PbTiO_3$ and $PbZr_{1-x}Ti_xO_3$ systems is typically p-type and mediated by lead-site defects (hole conduction attributed to lead vacancies, Pb^{3+} centers, or impurities) (Supporting Information).[33–38] These mobile holes lead to a lowering of the electrical resistivity and poor ferroelectric performance. Prior work has identified a shallow hole trap with an activation energy of ≈0.26 eV which has been attributed to Pb^{3+}

© 2016 WILEY-VCH Verlag GmbH & Co. KGaA, Weinheim

centers.[35,39] Furthermore, the ionization level of lead vacancies has been calculated to be 0.56 eV from the top of valence band[36] and an acceptor level located 0.39 eV above valance band edge has been measured in $PbZr_{1-x}Ti_xO_3$.[40] Additionally, although oxygen vacancies are also present and compensate some (or most) of the holes (thus weakening the p-type conduction), oxygen vacancy-related defects are thought to be relatively deep donors[36] limiting the potential for n-type conduction (which is consistent with the fact that n-type conductivity is less frequently observed in $PbTiO_3$ systems, even at low oxygen pressures).[33,34,36,41,42] Finally, studies have indicated that Ti^{3+} centers can also be present and act as deep electron traps located 1 eV or more below the conduction band edge.[35,37,38,43] Thus, we conclude that the transport in the high-pressure O_2 heterostructures is dominated by Pb^{3+} centers (trap energy of 0.25–0.27 eV), that in the low-pressure O_2 heterostructures it is dominated by lead vacancies (trap energy of 0.46–0.50 eV), and that in the He^{2+} bombarded, high-pressure O_2 heterostructures it is dominated by a much deeper state (trap energy of 0.93–1.01 eV) which is most likely associated with deep lying defect complexes, although the energy also matches with the values reported for Ti^{3+} centers.

What all of these data come together to reveal is that producing the "best" material (in this case a material with high crystallinity and nearly ideal stoichiometry) does not necessarily result in the ideal properties. In particular, in $PbTiO_3$, such high-pressure O_2 heterostructures are dominated by the presence of isolated point defects, namely Pb^{3+} and lead vacancies (as detected by DLTS and *I–V*), which give rise to readily activated shallow trap states and, in turn, enhanced hole conduction and poor ferroelectric performance. Upon either in situ or ex situ bombardment, the production of higher concentrations of defects results in the production of deeper trap states associated with defect complexes. In the low-pressure O_2 heterostructures, the data suggest that all trap states associated with shallow Pb^{3+} centers are quenched, but that some trap states associated with lead vacancies (which occurred in much higher concentrations even in the high-pressure O_2 heterostructures) remain. In the He^{2+} bombarded, high-pressure O_2 heterostructures, the more aggressive introduction of defects results in in complete quenching of both the trap states associated with the Pb^{3+} and lead vacancies, and thus a dramatic reduction of the conductivity of the films. Besides impacting the trap states available in the material, the defects/disorder induced by the in situ or ex situ bombardment could also have the added benefit of lowering the carrier mobility (via lattice, defect, and impurity scattering). All told, the combined effects manifest themselves as a ≈5 order of magnitude reduction of leakage current. We also note that earlier work on low-energy oxygen-ion bombardment of ferroelectrics[44–46] also showed the potential to control ferroelectric properties. This early work, however, did not delve into the mechanism for the improved properties and perhaps the current work begins to better explain these observations and provide a framework by which additional control of materials can be produced.

In conclusion, our experimental observations show that the growth of high-quality thin films does not necessarily lead to optimum properties. We have demonstrated that even small concentrations of defects present in these films, which are hard-to-detect using conventional techniques such as X-ray diffraction, can dramatically affect the properties. The defects responsible for poor transport and ferroelectric properties in $PbTiO_3$ thin films are identified to be isolated point defects such as Pb^{3+} centers and lead vacancies, which contribute to hole conduction. Introduction of bombardment-induced defects is shown to be an effective way to quench these trap states by turning them into deep lying defect complexes and clusters which, in turn, leads to a dramatic reduction of leakage current by up to 5 orders of magnitude and improvement of ferroelectric device performance.

Experimental Section

Heterostructure Growth: Heterostructures were grown via pulsed-laser deposition using a KrF excimer laser (248 nm, LPX 300, Coherent), in an on-axis geometry with a 60 mm target-to-substrate spacing. Films were grown on $SrTiO_3$ (001) single-crystal substrates (Crystec, GmbH) from ceramic targets with chemistries $SrRuO_3$ and $Pb_{1.1}Ti_{1.0}O_3$. Targets were sanded, cleaned, and sufficiently preablated prior to every growth to assure the target surface had reached steady state prior to film deposition. The $SrRuO_3$ bottom electrodes were grown at a heater temperature of 690 °C in a dynamic oxygen pressure of 100 mTorr at a laser repetition rate of 14 Hz and a laser fluence of 1.3 J cm^{-2}. The $PbTiO_3$ films were grown at a heater temperature of 675 °C in a dynamic oxygen pressure of 200 mTorr (high-pressure) or 50 mTorr (low-pressure) at a laser repetition rate of 15 and 2 Hz, respectively (in order to maintain the cation ratio as close as possible to the stoichiometric composition) while maintaining the laser fluence to be 1.9 J cm^{-2}. A third variant of $PbTiO_3$ film was grown at a total pressure of 200 mTorr, but with a mixture of 50 mTorr of oxygen and balance Ar to explore the role of lower oxidative potential, but higher deposition pressures. All other conditions were the same as the 200 mTorr growth in pure oxygen. Following growth, the films were cooled down at a rate of 5 °C min^{-1}. to room temperature in an oxygen pressure of 700 Torr.

Chemical Analysis: Film chemistry was probed via RBS with an incident He-ion energy of 3040 keV, an incident angle $\alpha = 22.5°$, an exit angle $\beta = 25.35°$, and a scattering angle $\theta = 168°$ in the Cornell geometry. RBS samples were also grown on $SrTiO_3$ (001) substrates concurrently with the films studied herein. Following the measurements, modeling fits of the data were completed using the built-in fitting program in the RBS analysis software SIMNRA (simnra.com).

Transport and Ferroelectric Properties: Circular capacitors with radius of 50 microns were produced. Top $SrRuO_3$ electrodes were grown at 550 °C (in order to minimize lead-loss during processing) while all other conditions were the same as the bottom $SrRuO_3$ electrode growth following established procedure.[22] Ferroelectric hysteresis loops were measured using a Precision Multiferroic Tester (Radiant Technologies) at frequencies from 0.1 to 100 kHz. Transport properties were measured using a Keithley 6517B programmable electrometer over a temperature range of 300–470 K, in both positive and negative polarities, using an unswitched triangular voltage profile (in order to prevent any contributions from switching currents) with maximum ±3 V bias.

STEM Analysis: Cross-sectional TEM specimens were prepared by tripod mechanical polishing at an angle of 1° followed by low-angle argon-ion milling at 4 keV. The ion bombarded samples were glued to a pristine $SrTiO_3$ wafer prior to polishing to confirm that defects were not induced through the sample preparation process. HAADF-STEM and LAADF-STEM images were acquired on a F20 UT Tecnai operated at 200 keV.

Ion Bombardment: Ion bombardment was carried out in the Pellatron located at Lawrence Berkeley National Laboratory using He^{2+} ions with an energy of 3 MeV and incident angle $\alpha = 0°$ and exit angle $\beta = 12.00°$ in the Cornell geometry. A large aperture size (comparable to the size of the sample) was used in order to achieve a uniform irradiation dose across the entire surface of the heterostructure.

© 2016 WILEY-VCH Verlag GmbH & Co. KGaA, Weinheim

SRIM/TRIM Simulations: All simulations were made using SRIM 2013 (srim.org). SRIM is a group of programs which calculate the stopping and range of ions into matter using a quantum mechanical treatment of ion-atom collisions. TRIM is the most comprehensive program included in SRIM, which accepts complex targets made of compound materials with up to eight layers, and calculates final 3D distribution of the ions, target damage, sputtering, ionization, and phonon production.

Impedance Spectroscopy: Impedance spectroscopy is a powerful technique capable of differentiating between different contributions to the overall resistive response of a material. Impedance plots (imaginary vs real) can contain several semicircles wherein each semicircle is characteristic of a single time constant or transport mechanism. Presence of multiple semicircles in the complex impedance plane can be attributed to bulk and a grain-boundary response, presence of mixed conduction (i.e., both electronic and ionic), contribution from surface layers, or sample-electrode interfaces. Impedance measurements were performed using Gamry Instruments-Reference 600 potentiostat, under an oscillation voltage of 8 mV_{rms}, in a frequency range of 10 mHz–1 MHz.

DLTS: DLTS measurements were carried out using Precision Multiferroic Tester (Radiant Technologies), in a temperature range of 100–425 K with 5 K intervals, and 3 K min^{-1} ramp rate. The samples were kept for 5 min. at each temperature before measurement. A +5 V pulse of 10 ms duration was applied to the samples, and the corresponding DLTS signal was measured at the end of the pulse using the conventional rate-window approach.[30] The DLTS signal (difference in transient capacitance at two different times t_1 and t_2 after the filling pulse) was then plotted as a function of temperature for five different rate windows ranging from 5 to 160 ms. Shifting of DLTS peaks could be obtained by varying the rate windows.

Supporting Information

Supporting Information is available from the Wiley Online Library or from the author.

Acknowledgements

S.S. acknowledges support from the National Science Foundation under grant CMMI-1434147. R.X. acknowledges support from the National Science Foundation under grant DMR-1451219. L.R.D. acknowledges support from the U.S. Department of Energy, Office of Basic Sciences under grant no. DE-SC0012375 for chemical analysis of the films. Z.C. acknowledges support from the Air Force Office of Scientific Research under grant FA9550-12-1-0471 and from the Laboratory Directed Research and Development Program of Lawrence Berkeley National Laboratory under U.S. Department of Energy Contract No. DE-AC02-05CH11231 for the development of advanced synthesis methods. A.R.D. acknowledges support from the Army Research Office under grant W911NF-14-1-0104. L.W.M. acknowledges support from the National Science Foundation under grant OISE-1545907. Work at the Molecular Foundry and the National Center for Electron Microscopy was supported by the Office of Science, Office of Basic Energy Sciences, of the U.S. Department of Energy under Contract No. DE-AC02-05CH11231.

Received: July 26, 2016
Revised: September 1, 2016
Published online: October 10, 2016

[1] L. A. Girifalco, *Statistical Physics of Materials*, Wiley, New York, NY, USA **1973**.
[2] S. A. Campbell, *The Science and Engineering of Microelectronic Fabrication*, Oxford University Press, New York, NY, USA **2001**.
[3] *Handbook of Semiconductor Manufacturing Technology* (Eds: R. Doering, Y. Nishi), CRC Press, Boca Raton, FL, USA **2008**.
[4] E. G. Seebauer, K. W. Noh, *Mater. Sci. Eng. R* **2010**, *70*, 151.
[5] T. Suzuki, Y. Nishi, M. Fujimoto, *Philos. Mag. A* **2000**, *80*, 621.
[6] D. Damjanovic, *Rep. Prog. Phys.* **1998**, *61*, 1267.
[7] T. Ohnishi, K. Shibuya, T. Yamamoto, M. Lippmaa, *J. Appl. Phys.* **2008**, *103*, 103703.
[8] D. J. Keeble, S. Wicklein, R. Dittmann, L. Ravelli, R. A. Mackie, W. Egger, *Phys. Rev. Lett.* **2010**, *105*, 226102.
[9] E. Breckenfeld, R. Wilson, J. Karthik, A. R. Damodaran, D. G. Cahill, L. W. Martin, *Chem. Mater.* **2012**, *24*, 331.
[10] E. Breckenfeld, R. B. Wilson, L. W. Martin, *Appl. Phys. Lett.* **2013**, *103*, 082901.
[11] E. Breckenfeld, Z. Chen, A. R. Damodaran, L. W. Martin, *ACS Appl. Mater. Interfaces* **2014**, *6*, 22436.
[12] B. Jaffe, W. R. Cook, H. Jaffe, *Piezoelectric Ceramics*, Academic, New York, NY, USA **1971**.
[13] L. E. Cross, in *Ferroelectric Ceramics* (Eds: N. Setter, E. L. Colla), Birkhauser, Basel, Switzerland **1993**.
[14] X. Ren, *Nat. Mater.* **2004**, *3*, 91.
[15] D. Lee, B. C. Jeon, S. H. Baek, S. M. Yang, Y. J. Shin, T. H. Kim, Y. S. Kim, J.-G. Yoon, C.-B. Eom, T. W. Noh, *Adv. Mater.* **2012**, *24*, 6490.
[16] A. R. Damodaran, E. Breckenfeld, Z. Chen, S. Lee, L. W. Martin, *Adv. Mater.* **2014**, *26*, 6341.
[17] S. J. Pearton, *Mater. Sci. Rep.* **1990**, *4*, 313.
[18] Y. Takamura, R. V. Chopdekar, A. Scholl, A. Doran, J. A. Liddle, B. Harteneck, Y. Suzuki, *Nano Lett.* **2006**, *6*, 1287.
[19] H. Guo, S. Dong, P. D. Rack, J. D. Budai, C. Beekman, Z. Gai, W. Siemons, C. M. Gonzalez, R. Timilsina, A. T. Wong, A. Herklotz, P. C. Snijders, E. Dagotto, T. Z. Ward, *Phys. Rev. Lett.* **2015**, *114*, 256801.
[20] S. L. Morelhaoa, J. Z. Domagalab, *J. Appl. Cryst.* **2007**, *40*, 546.
[21] A. H. G. Vlooswijk, *Ph.D. Thesis*, Zernike Institute, Groningen, The Netherlands **2009**.
[22] J. Karthik, A. R. Damodaran, L. W. Martin, *Adv. Mater.* **2012**, *24*, 1610.
[23] T.-F. Tseng, M.-H. Yeh, K.-Sh. Liu, I.-N. Lin, *J. Appl. Phys.* **1996**, *80*, 4984.
[24] C. Wang, B. L. Cheng, S. Y. Wang, H. B. Lu, Y. L. Zhou, Z. H. Chen, G. Z. Yang, *Thin Solid Films* **2005**, *485*, 82.
[25] D. D. Perovic, C. J. Rossow, A. Howie, *Ultramicroscopy* **1993**, *52*, 353.
[26] S. E. Hillyard, J. Silcox, *Ultramicroscopy* **1995**, *58*, 6.
[27] D. A. Muller, N. Nakagawa, A. Ohtomo, J. L. Grazul, H. Y. Hwang, *Nature* **2004**, *430*, 657.
[28] A. R. West, D. C. Sinclair, N. Hirose, *J. Electroceram.* **1997**, *1*, 65.
[29] N. J. Donnelly, C. A. Randall, *Appl. Phys. Lett.* **2010**, *96*, 052906.
[30] D. V. Lang, *J. Appl. Phys.* **1974**, *45*, 3023.
[31] P. K. Giri, Y. N. Mohapatra, *Mater. Sci. Eng. B* **2000**, *71*, 327.
[32] M. Levinson, C. A. Aemiento, S. S. P. Shah, *Mater. Res. Soc. Symp. Proc.* **1987**, *92*, 353.
[33] R. Gerson, H. Jaffe, *J. Phys. Chem. Solids* **1963**, *24*, 979.
[34] V. V. Prisedsky, V. I. Shishkovsky, V. V. Klimov, *Ferroelectrics* **1977**, *17*, 465.
[35] J. Robertson, W. L. Warren, B. A. Tuttle, D. Dimos, D. M. Smyth, *Appl. Phys. Lett.* **1993**, *63*, 1519.
[36] Z. Zhang, P. Wu, L. Lu, C. Shu, *Appl. Phys. Lett.* **2006**, *88*, 142902.
[37] D. J. Wouters, G. J. Willems, H. E. Maes, *Microelectron. Eng.* **1995**, *29*, 249.
[38] D M Smyth, *Curr. Opin. Solid State Mater. Sci.* **1996**, *1*, 692.
[39] P. F. Baude, C. Ye, D. L. Polla, *Appl. Phys. Lett.* **1994**, *64*, 2670.
[40] T. P.-C. Juan, S.-M. Chen, J. Y.-M. Lee, *J. Appl. Phys.* **2004**, *95*, 3120.
[41] R. Gerson, *J. Appl. Phys.* **1960**, *31*, 188.
[42] B. A. Boukamp, M. T. N. Pham, D. H. A. Blank, H. J. M. Bouwmeester, *Solid State Ionics* **2004**, *170*, 239.
[43] C. Sudhama, J. Kim, J. Lee, V. Chikarmane, W. Shepard, E. R. Meyers, *J. Vac. Sci. Technol. B* **1993**, *11*, 1301.
[44] S. B. Krupanidhi, H. Hu, V. Kumar, *J. Appl. Phys.* **1992**, *71*, 376.
[45] H. Hu, S. B. Krupanidhi, *Appl. Phys. Lett.* **1992**, *61*, 1246.
[46] L. R. Zheng, P. X. Yang, L. W. Wang, C. L. Lin, S. C. Zo, *Nucl. Instrum. Methods Phys. Res. B* **1997**, *127/128*, 621.

© 2016 WILEY-VCH Verlag GmbH & Co. KGaA, Weinheim